
HEAT AND MASS TRANSFER
AND PHYSICAL GASDYNAMICS

Analysis of Three-Dimensional Turbulent Flow in an S-Shaped Rectangular Channel

A. V. Garbaruk, M. Kh. Strelets, and M. L. Shur

St. Petersburg State Technical University, St. Petersburg, 195251 Russia

Received June 13, 2002

Abstract—Three-dimensional Reynolds equations are used to calculate a turbulent flow in an S-shaped rectangular channel, which was experimentally investigated by Bruns *et al.* [1]. It is the main objective of these calculations to estimate the accuracy provided by the most popular linear models of turbulent viscosity in application to complex three-dimensional flows. In particular, two models of this type are treated, namely, the Menter model [2] and the Spalart-Allmaras model [3]. In addition, in order to estimate the possibility of improving the accuracy of simulation owing to the inclusion of the effect of curvature of the stream lines and of anisotropy of the Reynolds stress tensor, calculations are also performed using the appropriate modifications of the Spalart-Allmaras model [3], as suggested in [4, 5]. It is demonstrated that all of the treated models produce similar results, qualitatively correctly describe the experimentally observed tendencies, and, by and large, provide for an adequate qualitative agreement between the prediction and experimental data over the averaged characteristics of flow. Some differences are observed only downstream of the inflection point of the S-shaped walls, where a velocity profile with two-way downwash is realized. In calculating the Reynolds stresses, the nonlinear model of [5] is clearly advantageous over other models.

INTRODUCTION

Systematic studies into the possibilities of various semiempirical models of turbulence, initiated at the time of the first Stanford Conference [6], have resulted at present in setting certain “ratings” of such models, which characterize them both from the standpoint of exactness of calculation of various types of turbulent flows and from the standpoint of computational efficiency (see, for example, [7–9]). In particular, speaking of the simplest models based on the Boussinesq hypothesis of linear correlation between the tensors of Reynolds stresses and rates of deformation of averaged flow, the highest ratings (see, for example, [8]) are given to the k - ω model of Menter [2] (hereinafter referred to as M-SST model) and the Spalart-Allmaras model of turbulent viscosity transport (S-A) [3], as well as to the modification of the latter model allowing for the effects of curvature of stream lines and rotation (SARC) [4]. However, these ratings are mainly based on the results of calculations of two-dimensional wall flows, which is due to the limited base of experimental data on complex three-dimensional flows on the one hand, and to the laboriousness of calculations of such flows on the other hand. In view of this, the question of validity of these and other similar models for the calculation of complex three-dimensional flows characterized by a number of characteristic features (the presence of spatial pressure gradients and separation zones, significant anisotropy of turbulence) remains open, and special investigations are required for answering this question. At present, the solution of this problem

appears to be quite feasible owing to the advent of new methods of measuring the characteristics of turbulent flows and a considerable increase in the efficiency of computer equipment. In particular, in this paper we give the results of calculations of flow in an S-shaped rectangular channel (Fig. 1), which was experimentally investigated in detail by Bruns *et al.* [1]. Along with the results of measurements of the basic parameters of averaged flow in a three-dimensional boundary layer formed on flat (parallel to the xz plane) walls of the channel, data on the pulsation characteristics of flow are given in [1]. From the standpoint of estimating the capabilities of turbulence models, an important feature of this flow is the presence of both longitudinal and transverse (along the z axis) pressure gradients whose sign varies at the inflection point of the S-shaped walls of the channel (in the section with $x = 4.5$ m). This brings about the change of sign of the transverse component of velocity in the wall region of the boundary layer and, as a consequence, about a qualitative rearrangement of the velocity profile in the boundary layer. In particular, if the velocity profile has the so-called “one-way downwash” (angle between the velocity vector projection onto the xz plane and the x axis does not change its sign within the boundary layer) upstream of the inflection point of the channel, it is characterized by a “two-way downwash” (the foregoing angle remains positive in the external region of the boundary layer and becomes negative in its wall region) downstream of this point. Because of these features, this flow may be regarded as a fairly difficult and representative test for

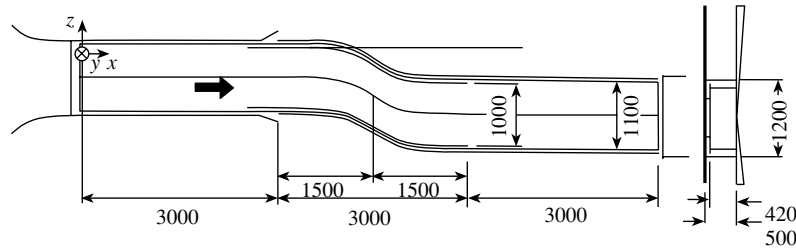


Fig. 1. The scheme of the experimental setup [1].

estimating the capabilities of semiempirical models of turbulence in calculating three-dimensional flows.

The calculations were performed within the Reynolds equations for incompressible liquid using the M-SST [2], S-A [3], and SARC [4] linear models of turbulent viscosity. Further, in order to assess the potential advantages of nonlinear models of turbulent viscosity, the nonlinear version of the SARC model [5] (SARCNL model) was treated, which is based on the following nonlinear correlation between the Reynolds stress tensor and the kinematic characteristics of averaged flow:

$$(\tau_{NL})_{ij} = \tau_{ij} - C_{NL}(\Omega_{ik}\tau_{ij} + \Omega_{jk}\tau_{ik}).$$

Here, τ_{NL} is the sought (nonlinear) vector of Reynolds stresses, τ is the Reynolds stress tensor determined using the classical Boussinesq linear hypothesis ($\tau_{ij} = -2\nu_t S_{ij}$), ν_t is the turbulent viscosity, Ω_{ik} is the normalized tensor of vorticity $\Omega_{ik} = \left(\frac{\partial u_i}{\partial x_k} - \frac{\partial u_k}{\partial x_i} \right) / \sqrt{\frac{\partial u_m}{\partial x_n} \frac{\partial u_m}{\partial x_n}}$, and C_{NL} is an empirical constant equal to 0.3 [5].

FORMULATION OF THE PROBLEM AND CALCULATION METHOD

As was already mentioned, the subject of investigation in the experiments of Bruns *et al.* [1] was the boundary layer developing on a flat channel wall parallel to the xz plane (Fig. 1). In order to eliminate the effect of the boundary layers formed on the S -shaped side walls, these boundary layers were cut off at the inlet to the S -shaped portion of the channel located at a distance of 2.5 m from the beginning of the channel. As a result, the channel width in this section decreases from 1.1 to 1 m. In view of this, the flow was calculated in two stages.

In the first stage, in order to determine the boundary conditions at the inlet to the S -shaped portion of the channel, the flow in the inlet (straight) portion of the channel 2.5 m long, 1.1 m wide, and 0.42 m high was calculated. In so doing, in accordance with the conditions of the experiment, the Reynolds number for the length of 1 m and velocity U_0 at the channel inlet was taken to be 10^6 . The inlet (at $x = 0$) boundary conditions in this stage involved a uniform profile of longitudinal

velocity, and the transverse components of velocity were assumed to be zero. The no-slip ($u = w = 0$) and impermeability ($v = 0$) conditions were preassigned on the channel walls, and soft boundary conditions (linear extrapolation from the internal points of the region to the outlet boundary), at the channel outlet.

The characteristics of turbulence, which must be preassigned as the boundary conditions, depend on the model of turbulence employed. In particular, in the case of the S-A model and its modifications, the boundary conditions must be preassigned directly for turbulent viscosity, and, in the case of the M-SST k - ω model, for the kinetic energy of turbulence k and specific rate of its dissipation ω . The conditions were preassigned as follows.

Almost zero turbulent viscosity, $\nu_t/\nu = 2 \times 10^{-3}$, was preassigned in the main part of the channel inlet section in accordance with the conditions of the experiment. In order to simulate the rough portion of the wall used in experiments for the turbulization of the boundary layer at the very beginning of the experimental section, a sinusoidal profile of turbulent viscosity with the maximal value of $\nu_t/\nu = 1$ was preassigned in the thin wall part of the flow. The turbulent viscosity on the channel walls was assumed to be zero; on the outlet boundary of the calculation region, soft boundary conditions were preassigned for ν_t/ν , as well as for velocity.

In accordance with the recommendations of Menter [2], the value of ω at the channel inlet was taken to be constant and equal to $10 \times (U_0/L)$ (where L is the channel width equal to 1.1 m), and the kinetic energy of turbulence was calculated by the formula $k = \omega \nu_t$ using the above-described profile of turbulent viscosity. The conditions of [2] were preassigned on the walls, namely, $k = 0$, $\omega = 60\nu/(\beta \Delta y_1^2)$, where $\beta = 0.075$, and Δy_1 is the grid spacing at the wall; on the outlet boundary, soft boundary conditions were preassigned, as for all other variables.

The results of solution of the problem described above using all of the treated models of turbulence turned out to be almost identical to one another and to agree well with the data of measurements of velocity in the flow core, as well as of friction and pressure on a flat wall in the channel section with $x = 1.9$ m, where the first measuring station is located. This points to the

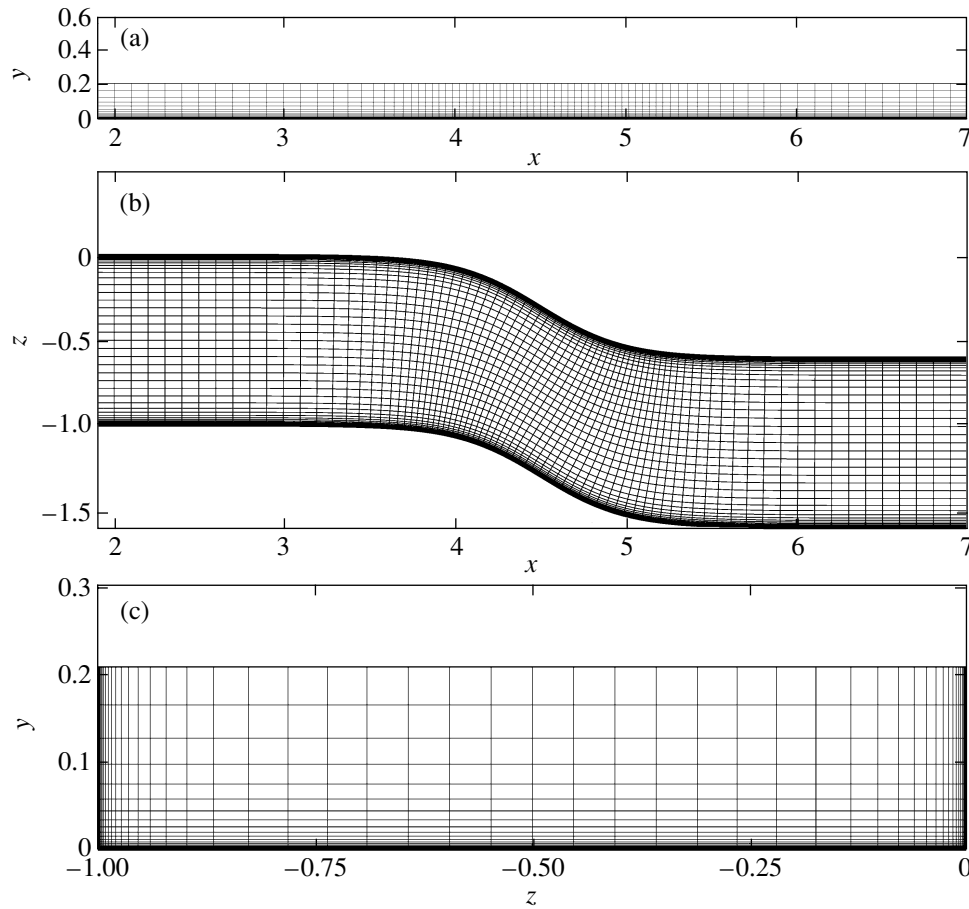


Fig. 2. (a, b) The scheme of the calculation region and (c) the grid used to calculate the flow in an *S*-shaped section of the channel (in the second stage of calculation).

absence of appreciable effect of variation of the channel width at $x = 2.5$ m and of its bend further downstream on the parameters of flow in the section with $x = 1.9$ m. As a result, the profiles of velocity and characteristics of turbulence in this section, obtained in the first stage of calculation, may be used as the inlet boundary conditions for the second stage, i.e., in calculating the flow directly in the *S*-shaped section of the channel. In order to simulate the “cutting off” of the boundary conditions on the *S*-shaped walls, which was performed in experiments in the section with $x = 2.5$ m, these profiles were “cut” in the sections with $z = 0.05$ m and $z = 1.05$ m. In order to eliminate the increase in the boundary layers on the *S*-shaped walls in the region from the inlet to the calculation region ($x = 1.9$ m) to the beginning of the *S*-shaped section ($x = 2.5$ m), the boundary conditions of free slip $\partial u/\partial z = 0$, $\partial v/\partial z = 0$, $w = 0$ were preassigned, and, at $x > 2.5$ m, the conditions of no-slip and impermeability $u = v = w = 0$ were preassigned. The respective calculation region and the calculation grid are shown in Fig. 2 (in view of the symmetry of flow relative to $y = 0.21$ m, the calculation region includes only half the channel). The rest of the boundary conditions on the walls and the conditions at

the outlet from the calculation region coincided with the above-described boundary conditions employed in the first stage of calculations.

In solving both problems, an implicit upwind differencing scheme [10] was used for numerical integration of Reynolds equations. The convection terms of the input equations were approximated by directional (upwind) differences with third-order accuracy, and the diffusion terms, by central differences with second-order accuracy. The resultant finite-difference equations were solved at each iteration using the Gauss-Seidel method with relaxation over planes.

The main series of calculations involved the use of the orthogonal nonuniform grid shown in Fig. 2. It had the dimensions $80 \times 35 \times 81$ in the x , y , and z directions, respectively, with the points crowded in the neighborhood of the walls in geometric progression with a coefficient of 1.3 or less. The first (wall) grid spacing in the wall law coordinates $\Delta y_1^+ = (\Delta y_1 v^*)/v$ did not exceed 1.0. The results of some calculations performed on a finer ($111 \times 47 \times 113$) grid of similar structure have demonstrated that the basic grid provides for an almost convergent solution.

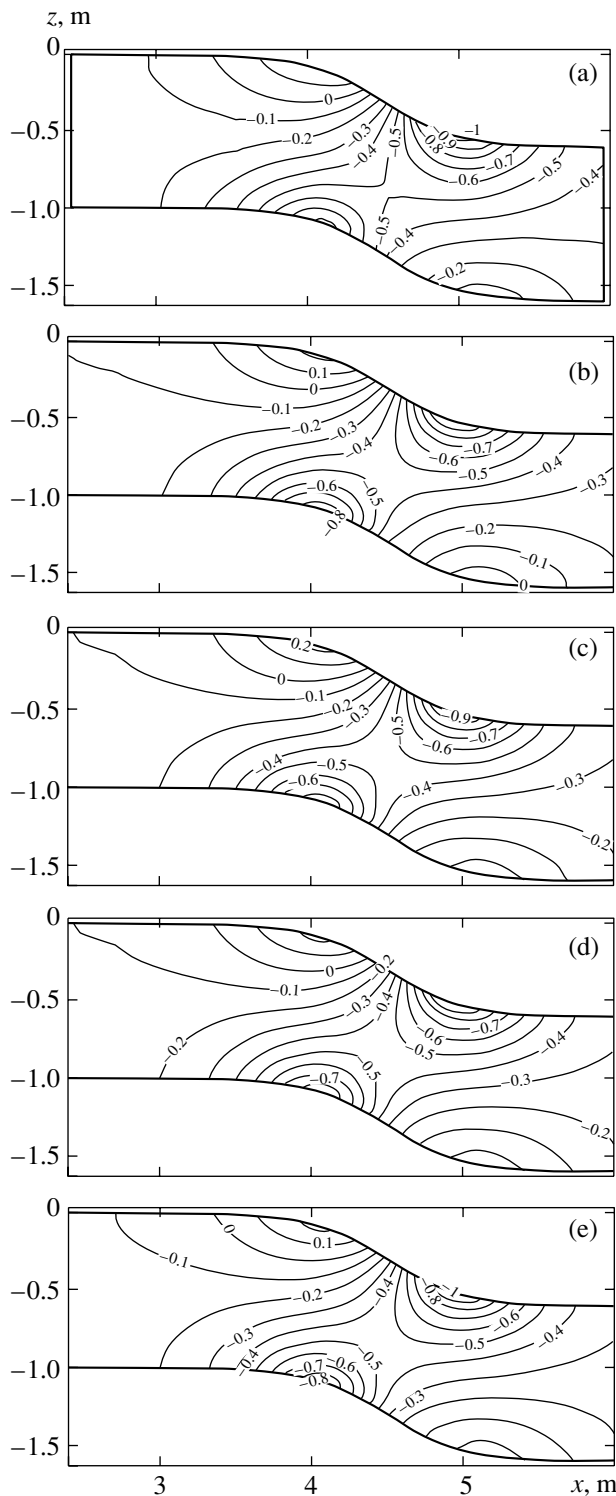


Fig. 3. Isolines of the pressure coefficient C_p on a flat wall of the channel: (a) experimental data, (b) calculation by the M-SST model [2], (c) S-A [3], (d) SARC [4], (e) SARCNL [5].

DISCUSSION OF THE RESULTS

Figure 3 gives the experimental fields of the pressure coefficient on a flat channel wall and the respective

results of calculations using four models of turbulence being treated. One can see that all models produce similar results and qualitatively correctly describe the experimentally observed behavior of pressure, including the variation of the sign of transverse (along the z axis) pressure gradient in the neighborhood of the inflection point of the side walls of the channel (at $x = 4.5$ m). A clearer quantitative view of the degree of agreement between the predicted and experimentally obtained distribution of pressure, as well of friction on the flat surface being treated, is given by Fig. 4. The figure shows the distribution of the coefficients of pressure $C_p = 2[p(x, z) - p_{\text{ref}}]/\rho U_{\text{ref}}^2$ and friction $C_f = 2\tau_w(x, z)/\rho U_{\text{ref}}^2$ (p_{ref} and U_{ref} denote the pressure and velocity at the channel inlet) along three lines located on this surface in parallel with the S -shaped side walls of the channel (the middle line M and two lines spaced 0.19 m upward (U) and downward (D) of this line on the z axis) where the measurements were performed. One can see in Fig. 4 that all four models predict almost identical distributions of the pressure coefficient and very close distributions of friction. Note that the advantage of the M-SST and SARCNL models over the S-A and SARC models is insignificant. This result is quite unexpected, because even in calculating simpler two-dimensional boundary layers with a longitudinal pressure gradient [8, 9], the difference between the distributions of friction calculated using the M-SST and S-A models is much more pronounced. The similarity of results obtained using all of the treated models is observed for the remaining parameters of averaged flow. In view of this, only the results obtained using the M-SST model are given. Note that, within the first “bend” of the channel (up to the section with $x \approx 4.2$ m), the calculation results are in very good agreement with experiment. However, further downstream, the predicted C_p and C_f curves deviate somewhat from the experimental data, although the pattern of predicted distributions of pressure and friction continues to reflect all of the singular features of their behavior in experiment.

As was noted in the introduction, the distinguishing feature of the flow being treated is the qualitative rearrangement of the velocity profile in the boundary layer when passing the middle of the S -shaped part of the channel. In Fig. 5, this rearrangement is characterized by predicted and experimentally obtained distributions of the angle β formed between the projection of the velocity vector on the xz plane with the x axis on the external boundary of the boundary layer, of the corresponding angle on the wall α_w , and of their difference ($\alpha_w - \beta$). The value of α_w was determined in the calculation, as in experiment, by the parameters of flow at a point with the coordinate $y_1^+ \approx 3$. Given in Fig. 5 for comparison is a variation of the slope of the S -shaped wall to the x axis. One can see in the figure that the predicted distribution of β is in good agreement with

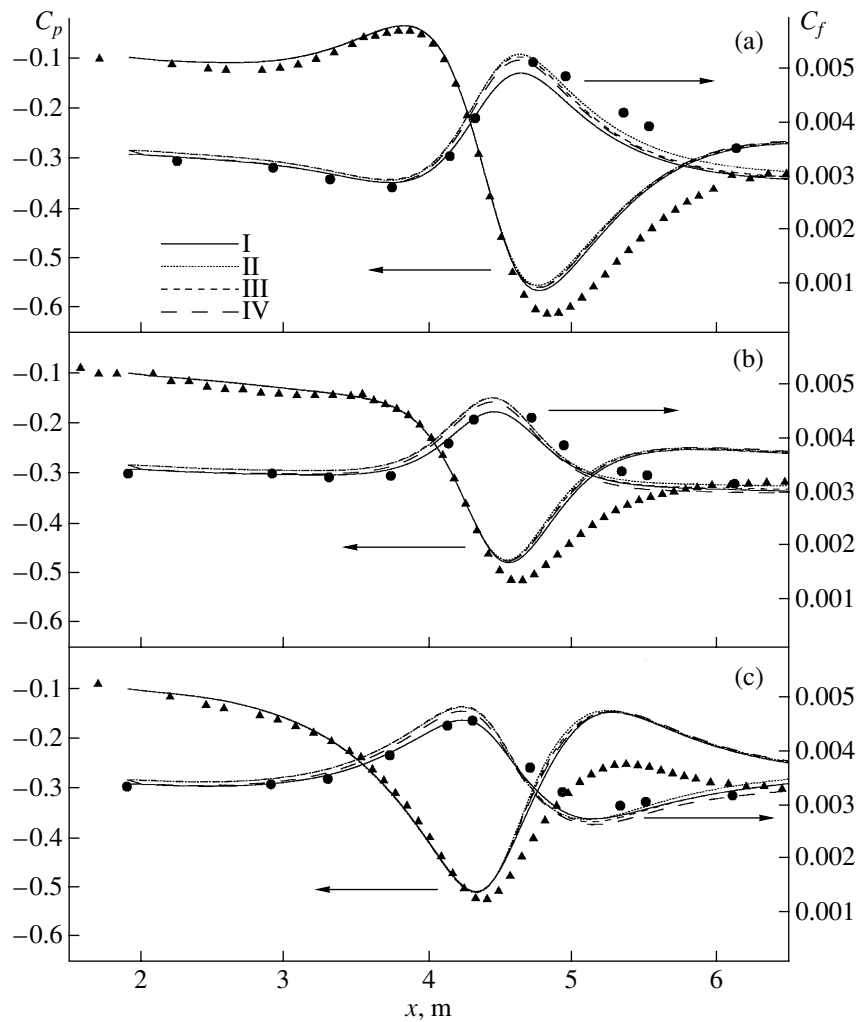


Fig. 4. The distribution of the coefficients of pressure C_p and friction C_f along the lines (a) U , (b) M , and (c) D . The points indicate the experiment [1]; I, calculation by the M-SST model [2]; II, S-A [3]; III, SARC [4]; IV, SARCNL [5].

experiment throughout the channel. The distribution of α_w , similarly to pressure and friction on the wall (Fig. 3), gradually deflects from the experimental points in the region downstream of the inflection point of the side walls of the channel; at the channel outlet, the difference between the prediction and experimental data for α_w may be as great as 4–5 degrees. The pattern of variation of the local angle of downwash ($\alpha - \beta$) across the boundary layer is shown in Fig. 6, which gives the predicted and experimentally obtained dependences on the universal coordinate y^+ at the point lying on the line M at $x = 4.925$ m. One can see in Fig. 6 that the difference between the predicted and experimentally obtained data is observed only in the internal region of the boundary layer (at $y^+ < 10^3$).

In spite of the observed deviation of the predicted data on pressure and downwash angle of the flow from experiment, the profiles of the longitudinal (parallel to the plate surface) component of the velocity vector, constructed in the wall law variables $u^+(y^+)$, agree very

well with experiment throughout the channel. Figure 7 gives, by way of example, comparison of the predicted and experimentally obtained profiles on the line M at $x = 4.925$ m. Similarly to experiment, neither the three-dimensional pattern nor the variation of the sign of the transverse component of velocity in the wall region of flow leads to a marked deviation of the velocity profiles in the internal region of the boundary layer from a similar profile in a two-dimensional boundary layer on a flat plate $u^+ = (1/0.4)\ln(y^+) + 5.1$.

In order to explain the possible reasons for the difference between the predicted and experimentally obtained distributions of pressure and downwash angle of flow in the internal region of the boundary layer in the second half of the S -shaped section of the channel (see Figs. 4–6), the velocity field was analyzed in more detail. Given by way of example in Fig. 8 are fragments of the predicted field of the longitudinal component of velocity in different cross sections of the second half of the S -shaped section of the channel. One can see in the

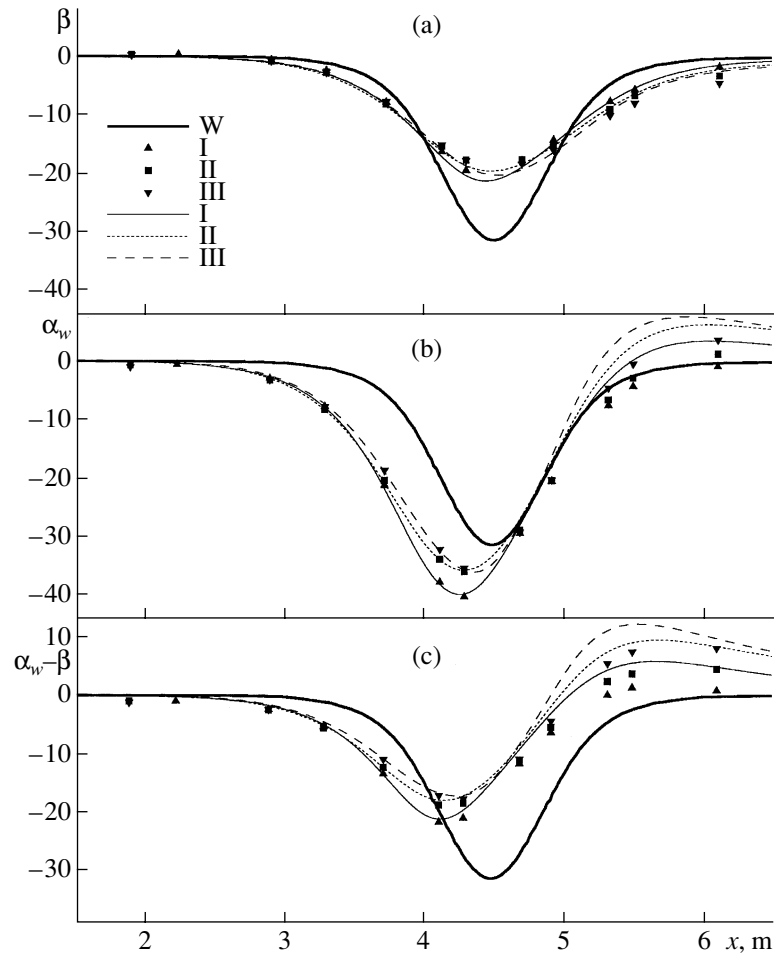


Fig. 5. The distribution of the angles (a) β , (b) α_w , and (c) their difference along the lines (I) U , (II) M , and (III) D ; W is the rotation angle of side walls. The points indicate the experiment, and the lines indicate the calculation by the M-SST model.

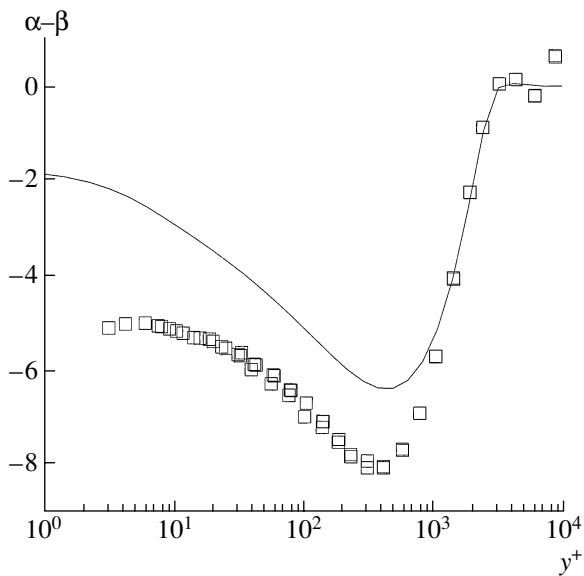


Fig. 6. The profile of the angle of downwash of the velocity profile on the line M at $x = 4.925$ m. The points indicate the experiment [1], and the line indicates the calculation by the M-SST model [2].

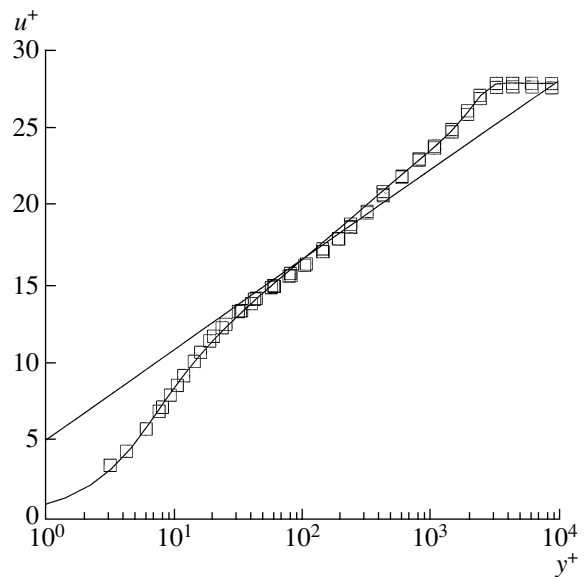


Fig. 7. The profile of the velocity component tangential to a flat wall in the wall law variables on the line M at $x = 4.925$ m. The points indicate the experiment [1], and the line indicates the calculation by the M-SST model [2].

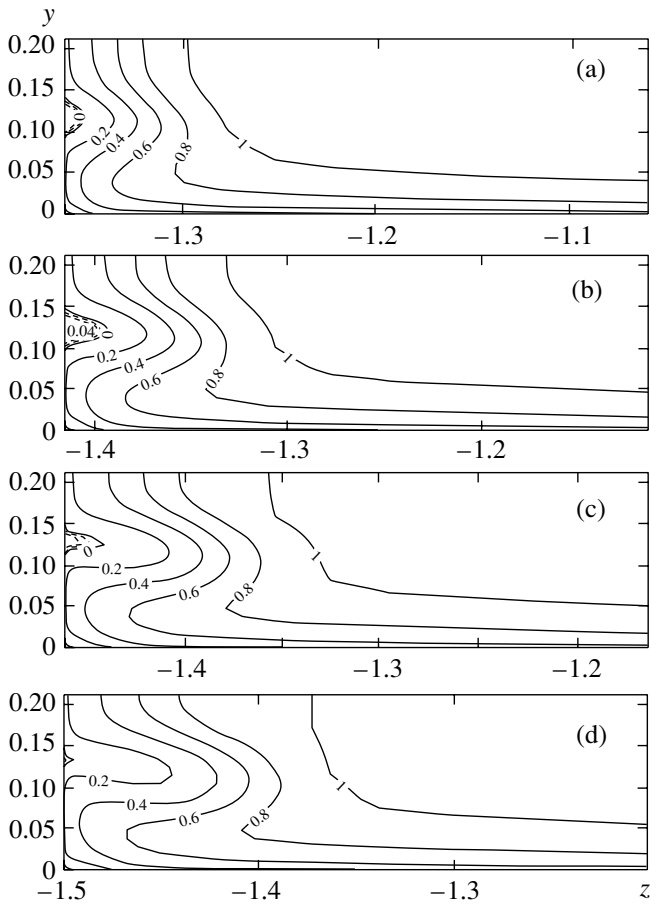


Fig. 8. Isolines of the longitudinal component of velocity in the channel cross section: (a) $x = 4.6$ m, (b) $x = 4.7$ m, (c) $x = 4.8$ m, and (d) $x = 4.9$ m. The calculation is performed by the SARC model [4].

figure that, according to the calculation, two (one in each of two channel halves symmetric with respect to y) small separation zones with the beginning at $x \approx 4.5$ m and the end at $x \approx 5.0$ m are formed on the lower S -shaped

wall. Unfortunately, no measurements were performed in this region during experiment; therefore, it is difficult to say how accurately the employed models of turbulence predict the size of the separation zone shown in Fig. 8. However, if we assume that they are underestimated, this will help explain the discrepancies between theory and experiment observed above, in particular, the overestimated pressure and underestimated friction on the flat wall in the second half of the S -shaped section of the channel.

On summing up all of the results treated above, it is possible to conclude that the employed modes of turbulence enable one to fairly accurately predict the principal averaged characteristics of the flow being treated and that the observed discrepancies between theory and experiment in the second part of the channel are apparently due to the inadequately accurate description of closed three-dimensional separation “bubbles” formed on the lower S -shaped wall of the channel.

The exactness of calculation of Reynolds stresses may be judged from Fig. 9, which gives the predicted and experimentally obtained profiles of different components of the Reynolds stress tensor in the boundary layer on the line M in the cross section with $x = 4.925$ m. It follows from Fig. 9 that all of the treated models predict almost identical profiles of components $\overline{u'v'}$ and $\overline{v'w'}$ which agree with experiment at least qualitatively. At the same time, the $\overline{u'w'}$ profile may be qualitatively correctly described (though with a serious error) only using the nonlinear SARCNL model. However, one can see from the foregoing results that this does not entail a marked increase in the accuracy of calculation of the characteristics of averaged flow. Therefore, the obtained results support the thesis that it is not always that improvements in the quality of description of Reynolds stresses guarantee improvements in the quality of description of the characteristics of averaged flow [5].

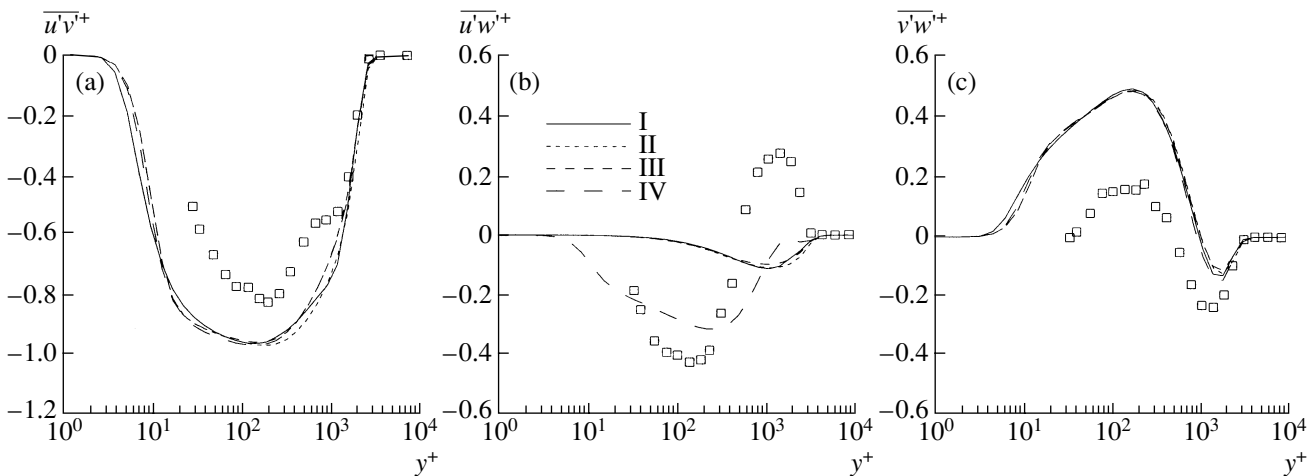


Fig. 9. Profiles of tangential Reynolds stresses on the line M at $x = 4.925$ m. The points indicate the experiment [1]; I, calculation by the M-SST model [2]; II, S-A [3]; III, SARC [4]; IV, SARCNL [5].

CONCLUSIONS

The basic inference to be made from the calculation results is that the high ratings of the S–A and M–SST models of turbulence, which are based on the results of calculations of two-dimensional boundary layers, by and large remain valid in analyzing much more complex three-dimensional flows. In particular, in calculating the flow in an S-shaped channel treated in this paper, both these models produce almost similar results which agree qualitatively and quantitatively with the experimental data on the characteristics of averaged flow. As to the treated modified versions of the S–A model, which take into account the effect of curvature of the stream lines on turbulence (SARC model) and the nonlinearity of correlation between the tensors of Reynolds stresses and rates of deformation (SARCNL), these effects hardly show up in the given flow. Some advantage of the latter model is observed only when calculating one of the components of the Reynolds stress tensor ($\overline{u'w'}$), which does not involve any appreciable increase in the accuracy of calculation of the averaged flow parameters.

Note further that a considerable discrepancy between the prediction and experimental data on pressure and downwash angle of flow in the internal region of the boundary layer is observed in the region of two-way downwash of the velocity profile in the boundary layer ($x > 4.5$ m); this discrepancy is apparently due to the inadequately accurate description of the closed separation region formed above the lower S-shaped wall of the channel.

ACKNOWLEDGMENTS

This study was supported by the Russian Foundation for Basic Research (project no. 00-02-17184).

REFERENCES

1. Bruns, J.M., Fernholz, H.H., and Monkewitz, P.A., *J. Fluid Mech.*, 1999, vol. 393, p. 175.
2. Menter, F.R., Zonal Two-Equation k – ω Turbulence Models for Aerodynamic Flows, *AIAA Paper*, 1993, AIAA-93-2906.
3. Spalart, P.R. and Allmaras, S.R., A One-Equation Turbulence Model for Aerodynamic Flows, *AIAA Paper*, 1992, AIAA-92-0439.
4. Spalart, P.R. and Shur, M.L., *Aerosp. Sci. Technol.*, 1997, vol. 1, no. 5, p. 297.
5. Spalart, P.R., *Int. J. Heat Fluid Flow*, 2000, vol. 21, p. 252.
6. Coles, D.E. and Hirst, E.A., *Computation of Turbulent Boundary Layers-1968, AFOSR-IFP Stanford Conf.*, Stanford Univ. Press, Palo Alto, CA, 1969, vol. II.
7. *European Computational Aerodynamics Research Project: Validation of CFD Codes and Assessment of Turbulence Models*, Haase, W., Chaput, E., Elsholz, E., *et al.*, Eds., *Notes on Numerical Fluid Mechanics (NNFM)*, 1997, vol. 58.
8. Garbaruk, A.V., Current Semi-Empirical Models of Turbulence for Wall Flows: Testing and Comparison, *Cand. Sci. (Phys.-Math.) Dissertation*, St. Petersburg: St. Petersburg State Univ., 1999.
9. Garbaruk, A.V., Lapin, Yu.V., and Strelets, M.Kh., *Teplofiz. Vys. Temp.*, 1998, vol. 36, no. 4, p. 607 (*High Temp.* (Engl. transl.), vol. 36, no. 4, p. 583).
10. Rogers, S.E. and Kwak, D., An Upwind Differencing Scheme for the Time-Accurate Incompressible Navier-Stokes Equations, *AIAA Paper*, 1988, AIAA-88-2583-CP.